

Research article

# Application and Optimization of 3D Dendritic TiO<sub>2</sub> in Water Disinfection Processes

You Wu<sup>1</sup>

\*\*Raffles Institution, 1 Raffles Institution Lane Singapore 575954

E-mail: [norman.wu@mohh.com.sg](mailto:norman.wu@mohh.com.sg)

---

## Abstract

This paper reports the performance of bacterial disinfection using 3D dendritic titanium dioxide with nanoribbon structures (3DD-TiO<sub>2</sub>), which is newly developed by the researchers. Characterization of 3DD-TiO<sub>2</sub> using SEM and TEM shows that the diameter of nanoribbons is nearly 18 nm only, resulting in an aspect ratio of more than 50. The hierarchical porous structure of the 3DD-TiO<sub>2</sub> would greatly favor the improvement of photocatalytic activity via enlarging the specific surface area. In comparison with the same-sized microspheres and commercial Degussa P25, which are both spherically structured, 3DD-TiO<sub>2</sub> displays a consistently better performance under the tested environment. Without UV illumination, the removal efficiency of *E.coli* by 3DD-TiO<sub>2</sub> is 6.4% and 8.7% higher than that of microspheres and P25, respectively. Under UV radiation, the disinfection kinetic constant *k* of the disinfection reaction using 3DD-TiO<sub>2</sub> is 23.2% and 33.9% higher than that of using microspheres and P25, respectively. A series of optimization studies have been carried out to identify the optimum operating parameters of a photocatalytic process using 3DD-TiO<sub>2</sub>. The results tend to suggest: a) optimum catalyst concentration is around 100mg/L; b) the optimum temperature for bacteria inactivation ranges between 10°C and 20°C; c) presence of humic acid and anions (SO<sub>4</sub><sup>2-</sup>) exhibits an inhibitory effect on water disinfection process; and d) cations (Ca<sup>2+</sup>) enhance the disinfection rate. These optimum operating parameters could be directly referenced for full-scale applications in future.

**Keywords:** Disinfection; Kinetics; Nanoribbon; Photocatalysis; TiO<sub>2</sub>

---

## 1 Introduction

---

<sup>1</sup> Email: [wuyou1132@gmail.com](mailto:wuyou1132@gmail.com)

The ever increasing standards for providing high-quality drinking water have put more stress on the removal of contaminants including pathogenic microorganisms. Conventional water treatment methods are typically chemical- and energy- intensive and incur high capital costs to build infrastructure for large-scale treatment. Moreover, intensive chemical processes such as using ammonia, hydrochloric acid, sodium hydroxide, ozone, permanganate and chlorine compounds generate treatment residuals that cause pollution and contamination of freshwater sources [1]. In recent years, a great amount of effort has been channeled into the research of photocatalytic disinfection of drinking water, which is considered a new method of cheap and low-energy disinfection. In particular, titanium dioxide ( $\text{TiO}_2$ ) has been identified as one of the most effective photocatalysts for disinfection due to a variety of factors, including low cost, non-toxicity, chemical stability and high effectiveness under ultraviolet light.

$\text{TiO}_2$  photocatalysts work via a strong oxidative process. Upon absorbing photons with energy equivalent or larger amount of energy than the band gap, photocatalysts form electron-hole pairs. For  $\text{TiO}_2$ , the band-gap ( $>3.0\text{eV}$  for rutile phase and  $>3.2\text{eV}$  for anatase phase) can be overcome with energy from photons from UV radiation which has a wavelength ranging from 10nm to 400nm, corresponding to photon energies from 3eV to 124eV. The electrons from the valence band will be excited into the conduction band, forming electron-hole ( $e^- h^+$ ) pairs in the  $\text{TiO}_2$  nanoparticle. These charge carriers may either recombine or react with electron donors and acceptors adsorbed onto the  $\text{TiO}_2$  surface. Positive holes in the valence band interact with water molecules to generate extremely reactive hydroxyl radicals which will then inactivate pathogens during the process of photocatalytic water disinfection [2]. The efficiency of the photocatalyst is dependent on the relative rate of recombination and reaction with electron donors and acceptors [3].

The photocatalytic activity of  $\text{TiO}_2$  depends greatly on the size, shape and surface structural morphology. Commercially available Degussa P25  $\text{TiO}_2$  has become a standard for scientific research because of a relatively well-defined nature (typically 70:30 anatase: rutile mixture) and superior photocatalytic activity than most other commercial  $\text{TiO}_2$ . More recently, nanomaterials have been found to possess superior biocidal properties due to their high specific surface area as well as their special shape and morphology [3]. This is supported by a recent study on antibacterial activity of single-walled carbon nanotubes (CNTs), which showed that the rate of cell death was directly related to the diameter of CNTs since direct contact with CNTs causes membrane damage and thus loss of cell viability [4]. Hence, it is reasonable to assume that the  $\text{TiO}_2$  nanoribbons with small diameter may have high toxicity to bacteria cells as well.

This work is aimed at achieving high efficiency bacterial inactivation using a novel 3D dendritic  $\text{TiO}_2$  microsphere with superfine nanoribbons, which have synergistic effect of shape-dependent antibacterial activity and photocatalytic disinfection property. The performance of 3DD- $\text{TiO}_2$ , in term of *E.coli*. removal efficiency, is assessed when it is applied into the photocatalytic disinfection process. The effects of temperature, organic and inorganic matters on 3DD- $\text{TiO}_2$  performance are also evaluated under various controlled test environments. This work could provide a promising alternative nanomaterial for water disinfection.

## 2 Materials and Methods

### 2.1 $\text{TiO}_2$ Nanomaterial Synthesis

The 3DD- $\text{TiO}_2$  nanostructures were synthesized through a hydrothermal process, according to the reported paper [5]. Briefly, proper amount of titanium isopropoxide (TTIP,  $>98\%$ , Sigma-Aldrich) and HCl was mixed in bottle A for 30 minute of stirring. After that, a certain amount of cetyltrimethyl ammonium bromide (CTAB, Sigma-Aldrich) was mixed with DI water in bottle B. After 30 minutes, bottle B was added into bottle A and stirred for 1 h to form the aqueous TTIP solution. After stirring, a certain amount of TTIP solution and certain amount of ethylene glycol (EG, Sigma-Aldrich) were put into a 125 mL autoclave. The total volume of reaction solution was kept at 81 mL. The molar ratios of the starting materials of TTIP aqueous solution were  $100\text{H}_2\text{O}:7\text{HCl}:0.03\text{CTAB}:0.05\text{TTIP}$ . The molar ratio of TTIP aqueous solution to EG was 1:2. The hydrothermal reaction was carried out at  $150^\circ\text{C}$  for 20 h. The

product was collected, and washed with ethanol for 3 times, followed by drying at 80 °C for 24 h. The product was calcined at 550 °C for 2 h to remove any remaining organics. Big TiO<sub>2</sub> microspheres were synthesized as a control material with the molar ratio of TTIP aqueous solution to EG as 1:0. TiO<sub>2</sub> P25 was purchased from Degussa Company, also used as a control material.

## 2.2 Characterization of TiO<sub>2</sub> Nanostructures

The morphology and size of the nanostructures were determined by transmission electron microscopy (TEM) (JEOL 2010-H microscope) operating at 200 kV, and scanning electron microscopy (SEM) (JEOL 6340). The crystalline structures were obtained by X-ray powder diffraction (XRD) patterns measured using Shimadzu XRD-6000 X-ray diffractometer with monochromated high-intensity Cu K $\alpha$  irradiation ( $\lambda=1.5418\text{\AA}$ ), operated at 40 kV and 30 mA.

## 2.3 Bacterial Growth and Exposure

*E.coli* (K12) was chosen as the model bacteria for antibacterial activity tests. *E.coli* was cultivated in Luria-Bertani (LB) nutrient solution at 37 °C for 18 h to get the exponential growth phase. The cells were harvested by centrifugation and washed with saline solution (0.9% NaCl) to remove residual macromolecules. All glass apparatuses and solutions used in the experiments were autoclaved at 121°C for 20 min to ensure sterility.

## 2.4 Experimental Design

Bacterial cells were dissolved in saline solution containing 100  $\mu\text{g/mL}$  of TiO<sub>2</sub> samples (sonicated for 1h before use), with a final cell concentration around  $10^7$  cfu/mL. Disinfection reactions were carried out in 200mL glass beakers illuminated by a 5W UV-A lamp of intensity  $600\mu\text{W/cm}^2$  and homogenized by magnetic stirrers. After the disinfection reactions, samples were diluted with a gradient method and then applied uniformly on three LB culture medium plates per gradient solution. These plates were incubated at 37°C for 24 h. The colony forming units were counted and compared with control plates to calculate percentage of cell viability ( $C/C_0$ ).

### 2.4.1 Effect of Catalyst Concentration

Firstly, prior to any experimentation, an optimal concentration for bacterial disinfection for the photoreactor system must be determined to achieve the best possible disinfection efficiency. A comparison was made between the efficiency of various 3DD-TiO<sub>2</sub> concentrations under UV radiation for 40 minutes. 3DD-TiO<sub>2</sub> slurry was introduced to a 30mL aqueous NaCl suspension of  $10^7$ cpu/mL of *E. coli*. at various concentrations.

### 2.4.2 Effect of Nanostructure

The efficiency of disinfection activity of Degussa P25, microspheres and 3DD-TiO<sub>2</sub> were compared using disinfection reactions. Based on the optimal catalyst concentration, each type of TiO<sub>2</sub> photocatalyst was introduced at a fixed concentration of 100mg/L into the reaction slurry. Experiments were conducted both with and without UV radiation.

### 2.4.3 Effect of Temperature

To simulate different temperature conditions, the reaction beakers were maintained at various temperatures ranging from 10°C to 60°C using water baths. The same experiment was conducted for 3DD-TiO<sub>2</sub> and P25 for comparison.

#### 2.4.4 Effect of Organic Matter

Humic acid was added into the solutions to simulate the presence of organic matter in natural water. Humic acid was added at a concentration of 10ppm into the solution. The same experiment was conducted for 3DD-TiO<sub>2</sub> and P25 for comparison.

#### 2.4.5 Effect of Ions

Ca<sup>2+</sup> and SO<sub>4</sub><sup>2-</sup>, which are predominant ions present in natural waters, were added into the solutions to simulate natural conditions. A chemical analysis of surface water [6] found Ca<sup>2+</sup> and SO<sub>4</sub><sup>2-</sup> present at concentrations 24.85mg/L and 24mg/L respectively. CaCl<sub>2</sub> and Na<sub>2</sub>SO<sub>4</sub> were used as sources of Ca<sup>2+</sup> and SO<sub>4</sub><sup>2-</sup> ions.

### 3 Results

#### 3.1 Characterization

As observed from Figures 1a and 1b, the dimension of each 3DD-TiO<sub>2</sub> was around 2-3 μm, including strands of 1D nanoribbons grown on the central TiO<sub>2</sub> sphere. Each strand of nanoribbon has a length ranging from 500nm to 1.5μm and diameter of roughly 25nm. Further characterization was done using TEM to show images of an individual 3DD-TiO<sub>2</sub> (Figure 1f) and the image of one strand of TiO<sub>2</sub> nanoribbon at the edge of the spheres (Figure 1c). The overall dimensions of the 3DD-TiO<sub>2</sub> are the same as that observed by SEM images in Figures 1a-b, however, the exact diameter of the nanoribbon is nearly 18nm, which is smaller than that observed by SEM due to the metal coating in measurement. The aspect ratio of the TiO<sub>2</sub> nanoribbon is larger than 50, which allows for a much faster rate of electron transfer compared to microspheres and P25, thus enhancing the photocatalytic activity [7, 8]. Typical hierarchical structures can be observed for the 3DD-TiO<sub>2</sub> in which: the distances between different 3DD-TiO<sub>2</sub> are in the range of micrometer scale, while the distances between different strands of TiO<sub>2</sub> nanoribbons are in the range of nanometer scale. The hierarchical porous structure of the 3DD-TiO<sub>2</sub> would greatly favor the improvement of photocatalytic activity via enlarging the specific surface area, allowing more light reflection and multiple scattering inside the interior, and promoting the electron transfer along the long 1D nanoribbon [9, 10]. Meanwhile, Figure 1d shows the morphology of TiO<sub>2</sub> microspheres with size of 2-3μm, which is the same as the overall dimensions of our 3DD-TiO<sub>2</sub>, with smooth surfaces. Figure 1e shows the typical image of Degussa P25. The individual particle size of P25 is around 25nm, but with certain aggregation. These two kinds of TiO<sub>2</sub> are selected as control samples to monitor the shape-effect antibacterial activity of 3DD-TiO<sub>2</sub>.

X-ray diffraction was used to measure the crystal phase of the 3DD-TiO<sub>2</sub>. From the XRD patterns in Figure 2, the 3DD-TiO<sub>2</sub> has a standard rutile structure (JCPDS file no. 21-1276) [11, 12]. This can be attributed to the acidic precursor reaction solution during synthesis of the nanomaterial.

#### 3.2 Disinfection Efficiency of 3DD-TiO<sub>2</sub>

##### 3.2.1 Empirical Disinfection Mechanism and Kinetics

The kinetics of the reaction was based on a pseudo-first-order reaction kinetics as derived from the classical disinfection model of the Chick-Watson equation [13]

$$\ln \left( \frac{c}{c_0} \right) = -K[c]^n t \quad (1)$$

where  $\frac{c}{c_0}$  is the reduction in the concentration of bacteria,  $K$  is the disinfection kinetic constant,  $c$  is the concentration of the disinfecting agent at time  $t$ , and  $n$  is the reaction order. It is noted that under a constant supplied irradiation, the concentration of the disinfecting agent can be considered to be constant with time for a fixed catalyst concentration and photoreactor lamp setup. Henceforth, the disinfection kinetic constant,  $K$ , in Equation (1) can be simplified into a first-order disinfection kinetic constant,  $k$ , as below.

$$\ln\left(\frac{c}{c_0}\right) = -kt \quad (2)$$

All first-order disinfection kinetic constants,  $k$ , presented in this manuscript will be calculated by application of the classic Chick-Watson disinfection model.

### 3.2.2 Effect of Catalyst Concentration

Malato et al. (2009) [1] reported that during photocatalytic disinfection processes, initial bacterial inactivation rate increases when catalyst concentration of aqueous TiO<sub>2</sub> slurry increases up to an optimal catalyst concentration, whereby the disinfection rate becomes independent of the slurry concentration due to light screening effect. This optimal concentration has been found to depend on the irradiation system and the photoreactor geometry. Typically, for a reactor path length of several centimeters, as is the case for this paper, the optimal catalyst concentration varies in the range of several hundred milligrams per litre.

Figure 3 shows the *E. coli* count at 10 min intervals using different catalyst concentrations. The results were obtained using the colony counting method of *E. coli* growth on agar plates with serial dilution of each sample. The efficiency at 100mg/L is higher than at other concentrations, as evident from the faster decrease in cell viability. This could be attributed to the reduced percentage transmittance of UV radiation through the solution with an increase in catalyst concentration. As the amount of TiO<sub>2</sub> increases, the increase in photon-catalyst interaction is reduced, causing the rate of photocatalytic activity to approach a maximum value. As such, we can consider 100mg/L 3DD-TiO<sub>2</sub> to be the optimum catalyst concentration.

### 3.2.3 Effect of Nanostructure

As shown from Figures 4 and 5, nanoribbon particles are consistently more efficient in bacteria disinfection both with and without UV radiation. This shows that it is intrinsically more efficient due to its novel morphology. Under UV radiation,  $k = 0.0494 \text{ min}^{-1}$  using 3DD-TiO<sub>2</sub> compared to  $0.0401 \text{ min}^{-1}$  and  $0.0369 \text{ min}^{-1}$  using microspheres and P25 respectively. (Table 1) The 3DD-TiO<sub>2</sub> particles possess favourable photocatalytic characteristics compared to microspheres and commercial P25 due to the higher surface area to volume ratio. The constituent nanoribbons units attached to the central TiO<sub>2</sub> sphere allow for a much higher fraction of atoms to be located at the surface of the particle, hence there is a significantly faster rate of electron transfer, which improves the photocatalytic activity.

### 3.2.4 Effect of Temperature

The temperature of the photocatalytic system has a direct impact on the rate of adsorption and desorption of materials, however, current literature on the effect of temperature on photocatalytic activity is lacking. As evident from Figures 6 and 7, the rate of bacteria inactivation is fastest at 10°C for both P25 and 3DD-TiO<sub>2</sub>. There is a slight decrease in the rate from 20°C to 30°C to 45°C. The rate at 5°C approximates that of 20°C, however, due to electrical costs incurred in lowering the temperature, treatment at 20°C is preferred over at 5°C. At 60°C, many cells die quickly from the high temperature, thus giving rise to the low cell viability especially at the start. A controlled experiment conducted at 60°C without any TiO<sub>2</sub> shows similarly high rates of cell death, hence it can be deduced that the low bacteria viability is largely due to the high temperature instead of TiO<sub>2</sub> photocatalytic activity.

The optimum range can thus be deduced to be from 10°C to 45°C. S. Malato et al. reported that this could be attributed to the higher activation energy required at low temperatures such that desorption of the final product becomes the rate limiting step. On the other hand, at higher temperatures, the exothermic step of adsorption of reactants is not favoured, limiting the rate of reaction [1].

### 3.2.5 Effect of Organic Matter

Humic substances are generated from the decomposition of organic compounds and act as precursors to harmful disinfection by-products during bacteria disinfection by chlorination. They have also been reported to encourage regrowth of bacteria in the absence of residual disinfectant and are thus likely to have significant impact on the disinfection properties of TiO<sub>2</sub> [14]. As evident from Figure 8, the efficiency of bacteria disinfection is greatly decreased with the introduction of the acid for both P25 and 3DD-TiO<sub>2</sub>. The disinfection kinetic constant 3DD-TiO<sub>2</sub> drops from 0.0494 min<sup>-1</sup> to 0.0438 min<sup>-1</sup> in the presence of humic acid, an 11.3% decrease. (Table 1) However, it should be noted that 3DD-TiO<sub>2</sub> still remains more efficient than P25 regardless of the addition of acid.

Ng et al. (2010) [15] hypothesized that the effect of humic acid could be due to the competition for oxidizing species between humic acid and *E. coli* cells. Moreover, humic acid molecules have a large surface area that easily blocks off and intercepts UV radiation in the aqueous solution. They also reported that there is a decreased amount of radiation available for activating TiO<sub>2</sub> due to competition from humic acid molecules for adsorption of UV photons. Some of the reactive oxygen species (ROS) generated will also be used for degradation of humic acid instead of deactivating *E. coli* cells, further reducing the photocatalyst efficiency. ROS are generated when TiO<sub>2</sub> is exposed to UV radiation; accumulation of ROS may lead to oxidative stress, which causes deactivation of cells. A combination of the above factors is likely to cause the significant reduction in efficiency of TiO<sub>2</sub> in bacteria disinfection.

### 3.2.6 Effect of Ions

Based on Figure 9, Ca<sup>2+</sup> exerts a positive effect on photocatalytic disinfection, as shown from the exponential decline in cell viability over time. Ca<sup>2+</sup> is capable of enhancing TiO<sub>2</sub> adsorption onto bacteria cells and disinfection of *E. coli* [16, 17]. TiO<sub>2</sub> has a point of zero charge of 6.25, [18] therefore under neutral pH conditions, surface charge of the catalyst is negative. According to Li et al. [19] the cell surface charge of *E. coli* is negative at pH 7, hence the presence of cations adsorbed on the catalyst weakens its overall negative charge and reduces the repulsion of *E. coli*. Ca<sup>2+</sup> ion bridging [17] with TiO<sub>2</sub> enhances surface charge attraction of *E. coli* cells to the catalyst, which further promotes adsorption, thus leading to an increase in disinfection rate. *K* showed a 7.9% increase from 0.0494 min<sup>-1</sup> to 0.0533 min<sup>-1</sup>. (Table 1)

In contrast, SO<sub>4</sub><sup>2-</sup> was observed to inhibit the photocatalytic activity, leading to a 13.6% decrease in the value of *k* from 0.0494 min<sup>-1</sup> to 0.0427 min<sup>-1</sup>. (Table 1) It has been reported that SO<sub>4</sub><sup>2-</sup> can act as scavengers of h<sup>+</sup> and ·OH to produce SO<sub>4</sub><sup>·-</sup> radicals based on the following reactions: [20]



SO<sub>4</sub><sup>·-</sup>, also a strong oxidative radical, should in theory assist in photooxidation of *E. coli*. However, it is less reactive than the scavenged h<sup>+</sup> and ·OH radicals, [20] thus it has a net inhibitive effect on the photocatalytic reaction kinetic.

## 4 Discussion

3DD-TiO<sub>2</sub> has substantially higher photocatalytic activity compared to TiO<sub>2</sub> microspheres and commercially available P25 regardless of the physical conditions of the reactor. This can be attributed to the small size of the

nanoribbons, which allows for direct interaction between  $\text{TiO}_2$  and bacteria. Further bacteria cell death under UV irradiation is caused by damage of the cell wall due to attack by reactive hydroxyl radicals which are formed upon photoexcitation of  $\text{TiO}_2$  molecules. Leakage of cell content occurs, leading to disruption of essential cell function such as respiratory activity. Higher adsorption rates of bacteria cells onto  $\text{TiO}_2$  particles are facilitated by larger surface-area-to-volume ratios of the photocatalyst. It has been reported that adsorption rate is positively correlated with the bactericidal effect, thus 3DD- $\text{TiO}_2$  has faster efficiency due to its larger specific surface area [21].

This improved disinfection ability reduces the required concentration of reaction slurry and hence the amount of  $\text{TiO}_2$  needed for more effective water treatment. Costs of  $\text{TiO}_2$  production can be cut significantly, further cementing 3DD- $\text{TiO}_2$  as the most promising disinfectant and which is feasible in commercial application. For cost effectiveness and minimal electricity costs,  $\text{TiO}_2$  concentration of 100mg/L should be used and the treatment should be conducted between 10°C and 20°C. Concentrations higher than 100mg/L will yield minimal increases in efficiency. However, results will vary according to the photoreaction system pathway, as well as the amount of organic matter present in the water.

With the use of any nano-particles, there is a risk of nanoparticle contamination if particles are not properly recovered by post-treatment. The use of dendritic nanoribbons, however, allows the catalyst to be easily separated from the solution due to relatively large size of the central micro-sphere. Hall et al. [22] and Beydoun et al. [23] attempted the use of magnetism to help retain or recover the catalyst by attachment to magnetic particles. The addition of foreign material may decrease the disinfection efficiency compared to pure slurry reactors but contribute to better practicality overall [2]. Similar methods may be applied to the dendritic particles to facilitate post-treatment particle separation. With this, the dendritic particle retains the properties of a nano-particle which has superior disinfection properties, yet can be easily retrieved, preventing contamination.

There exist many other factors affecting the efficiency of water disinfection using 3DD- $\text{TiO}_2$ , including radiant flux, catalyst particle size, concentration of oxygen in aqueous solution and pH. To effectively harness the full potential of the novel dendritic nanoribbon structure, the combined effect of these factors must be fully investigated. The interdependency of these factors makes it all the more crucial to study the exact influence each exerts on the other. The size of aggregate nanoparticles in aqueous solutions, for instance, is affected by the pH, which then determines the capability of the reaction slurry in transmitting UV radiation throughout the solution [1]. For future research, the effect of these factors with regards to different morphologies of  $\text{TiO}_2$  particles under solar illumination [24] must be analyzed to provide both the scientific and commercial sectors with an accurate picture of the necessary details.

## 5 Conclusion

3D dendritic  $\text{TiO}_2$  microspheres with superfine 1D nanoribbons (3DD- $\text{TiO}_2$ ) was introduced as a novel material for water disinfection. Our results showed that this 3DD- $\text{TiO}_2$  have substantially higher photocatalytic activity compared to microspheres and commercialized P25 both in dark and UV-A irradiation conditions. This can be attributed to the synergetic effect of shape-dependent and high-efficient photocatalytic disinfection. The concentration of photocatalyst used must be optimized for cost effectiveness, while presence of organic substances and differences in temperature exert a significant impact on the disinfection rate. This implies that the settings of the process parameters should be carefully determined in applying 3DD- $\text{TiO}_2$  to water disinfection. The enhanced efficiency of the 3DD- $\text{TiO}_2$  will undoubtedly be useful for commercial applications, as well as trigger research into more novel nanostructures to further strengthen the position of  $\text{TiO}_2$  as one of the most promising photocatalysts.

## References

[1] S. Malato, P. Fernandez-Ibanez, M.I. Maldonado, J. Blanco, W. Gernjak. Decontamination and disinfection of water by solar photocatalysis: Recent overview and trends, *Catalysis Today* 147 (2009) 1–59.

- [2] O. K. Dalrymple, E. Stefanakos, M. A. Trotsb, D. Y. Goswamia, A review of the mechanisms and modeling of photocatalytic disinfection, *Applied Catalysis B: Environmental* 98 (2010), pp. 27–38.
- [3] X.B. Chen and S. S. Mao, Titanium Dioxide Nanomaterials: Synthesis, Properties, Modifications, and Applications, *Chem. Rev.* 107 (2007), pp.2891-2959.
- [4] S.B. Liu, W. Li, H. Lin, N. Fang, M. W. Chang, R. Xu, Y.H. Yang, and Y. Chen, Sharper and Faster “Nano Darts” Kill More Bacteria: A Study of Antibacterial Activity of Individually Dispersed Pristine Single-Walled Carbon Nanotube. *J. Am. Chem. Soc.*, 3 (12) (2009), pp.3891-3902.
- [5] Z.Q. Sun, J. H. Kim, Y. Zhao, F. Bijarbooneh, V. Malgras, Y.M. Lee, Y.-M. Kang and S.X. Dou, Rational Design of 3D Dendritic TiO<sub>2</sub> Nanostructures with Favorable Architectures. *J. Am. Chem. Soc.*, 133 (48) (2011), pp 19314–19317.
- [6] D.M. Alrousan, P.S.M. Dunlop, T.A. McMurray, and J.A. Byrne, Photocatalytic inactivation of E. coli in surface water using immobilized nanoparticle TiO<sub>2</sub> films. *Water Res.* 43 (2009), pp. 47–54 .
- [7] Z. Liu, D.D. Sun, P. Guo, and J.O. Leckie, One-step fabrication and high photocatalytic activity of porous TiO<sub>2</sub> hollow aggregates by using a low-temperature hydrothermal method without templates, *Chemistry-An European Journal* 13(6) (2007), pp.1851-1855.
- [8] L. Liu, Z.Liu, H. Bai, and D.D. Sun, Concurrent filtration and solar photocatalytic disinfection/degradation using high-performance Ag/TiO<sub>2</sub> nanofiber membrane. *Water Research* 46(4) (2012), pp. 1101-1112.
- [9] F.D. Fonzo, C.S. Casari, V. Russo, M.F. Brunella, A.L. Bassi, and C.E. Bottani, Hierarchically organized nanostructured TiO<sub>2</sub> for photocatalytic applications. *Nanotechnology*, 20 (2009), pp. 015604.
- [10] H. Bai, Z. Liu, and D.D. Sun, A hierarchically structured and multifunctional membrane for water treatment. *Applied Catalysis B: Environmental* 111-112, (2012), pp.571-577.
- [11] X. Feng, J. Zhai, and L. Jiang (2005) The fabrication and switchable superhydrophobicity of TiO<sub>2</sub> nanorod films. *Angew. Chem. Int. Ed.* 44, 5115-5118.
- [12] H. Bai, Z. Liu, and D.D. Sun, Hierarchically multifunctional TiO<sub>2</sub> nano-thorn membrane for water purification. *Chemical Communications* 46(35) (2010), pp. 6542-6544.
- [13] J. Maruga'n, R. van Grieken, C. Sordo and C. Cruz, Kinetics of the photocatalytic disinfection of Escherichia coli suspensions. *Appl. Catal B* 82 (2008) 27–36.
- [14] D. Van der Kooij, A. Visser and W.A.M. Hijnen (1982) Determining the concentration of easily assimilable organic carbon in drinking water. *J Am Water Works Assoc* 74:540–545.
- [15] J.W. Ng, X.W. Zhang, T. Zhang, J-Hg Pan, J-H A. Du and D.D. Sun, Construction of self-organized free-standing TiO<sub>2</sub> nanotube arrays for effective disinfection of drinking water. *J Chem Technol Biotechnol*, 85 92010), pp. 1061–1066.
- [16] X.Z. Li, C.M. Fan and Y.P. Sun, Enhancement of photocatalytic oxidation of humic acid in TiO<sub>2</sub> suspensions by increasing cation strength. *Chemosphere*, 48 (2002), pp. 453–460.
- [17] S.H. Yoon, H.L. Chung, K.J. Kim and Fane AG, Effect of calcium ion on the fouling of nanofilter by humic acid in drinking water production, *Water Res.*, 32 (1998), pp. 2180–2186.
- [18] R. Pelton, X. Geng and M. Brook, Photocatalytic paper from colloidal TiO<sub>2</sub> – fact or fantasy. *Adv Colloid Interface Sci.*, 127 (2006), pp.43–53.

- [19] J. Li and L.A. McLandsborough, The effects of the surface charge and hydrophobicity of Escherichia coli on its adhesion to beef muscle, *Int J Food Microbiol* 53 (1999), pp.185–193.
- [20] X.W. Zhang, Y. Wang and G. Li, Effect of operating parameters on microwave assisted photocatalytic degradation of azo dye X-3B with grain TiO<sub>2</sub> catalyst. *J.Mol.Catal. A: Chem* 237 (2005), pp.199–205.
- [21] G. Gogniat, M. Thyssen, M. Denis, C. Pulgarin, S. Dukan, The bactericidal effect of TiO<sub>2</sub> photocatalysis involves adsorption onto catalyst and the loss of membrane integrity, *FEMS Microbiol. Lett.* 258 (1) (2006), pp.18-24.
- [22] T. Hall, D.Y. Goswami, C.Y. Wu, A magnetically fluidized photocatalytic reactor system for water purification in space applications, in: *ASES Solar Conference, ASES, Reno, NV, 2002.*
- [23] D. Beydoun, R. Amal, G.K.C. Low, S. McEvoy, Novel photocatalyst: Titania-coated magnetite. Activity and photodissolution, *J. Phys. Chem. B* 104 (2000), pp. 4387–4396.
- [24] C. Han, M. Pelaez, V. Likodimos, A. G. Kontos, P. Falaras, K. O'Shea, and D. D. Dionysiou, Innovative Visible Light-activated Sulfur doped TiO<sub>2</sub> for Water Treatment, *Applied Catalysis B: Environmental, Applied Catalysis B:Environmental*, 107 (1/2) (2011) 77-87.

## List of Figures

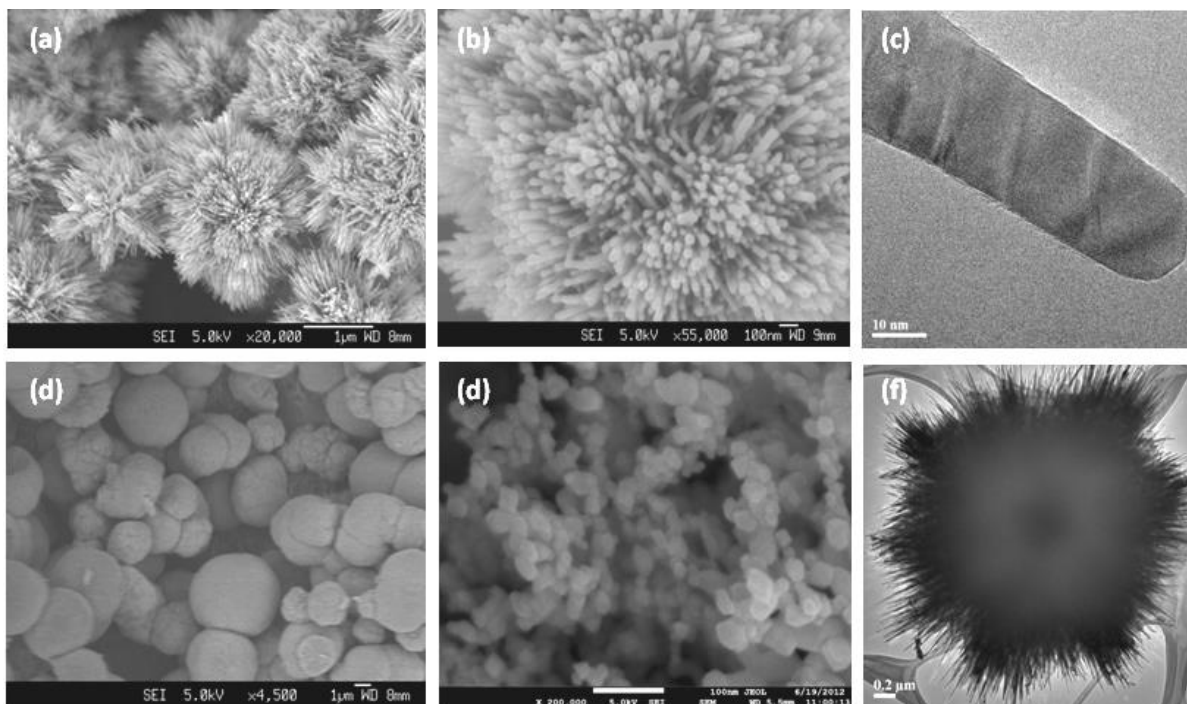


**Figure 1:** High-magnification SEM and TEM images of TiO<sub>2</sub> particles: (a) SEM image of 3DD-TiO<sub>2</sub>, (b) SEM image of strands of 1D nanoribbons grown on a 3DD-TiO<sub>2</sub>, (c) TEM image of an enlarged part of one strand of TiO<sub>2</sub> nanoribbon, (d) SEM image of TiO<sub>2</sub> microspheres, (e) SEM image of Degussa P25, (f) TEM image of an individual hierarchical 3DD-TiO<sub>2</sub>.

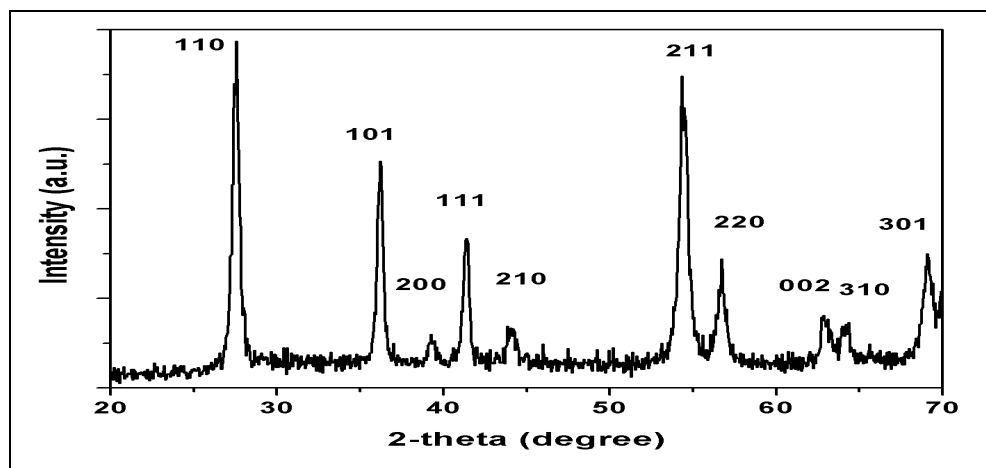


**Figure 2:** XRD patterns of the synthesized hierarchical 3DD-TiO<sub>2</sub> nanoribbon spheres.

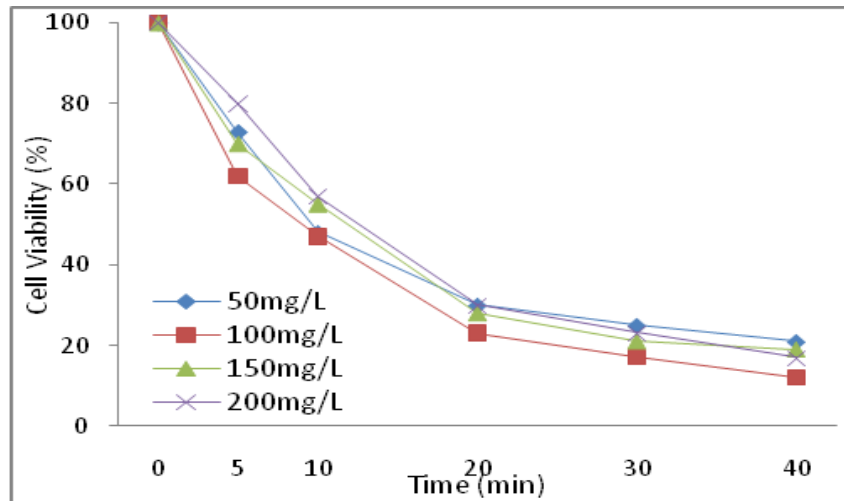


Figure 3: UV spectrophotometry results of treatment using various concentrations of 3DD-TiO<sub>2</sub>.

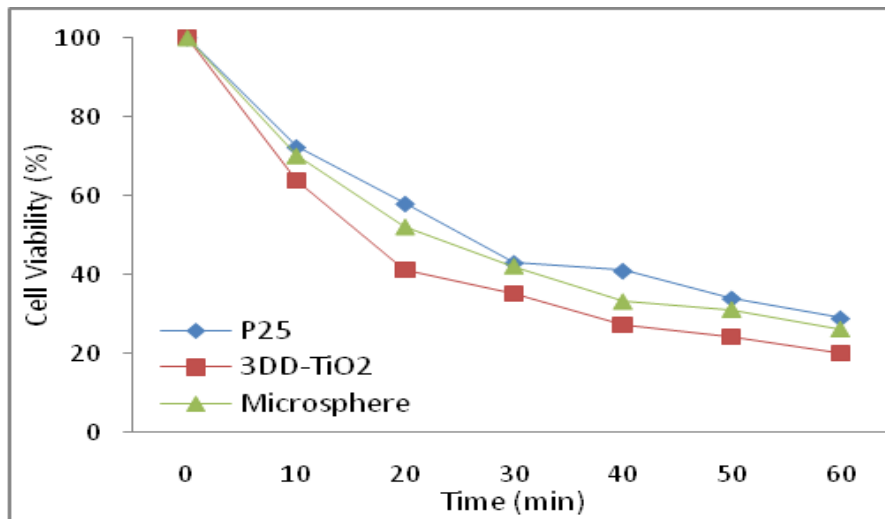
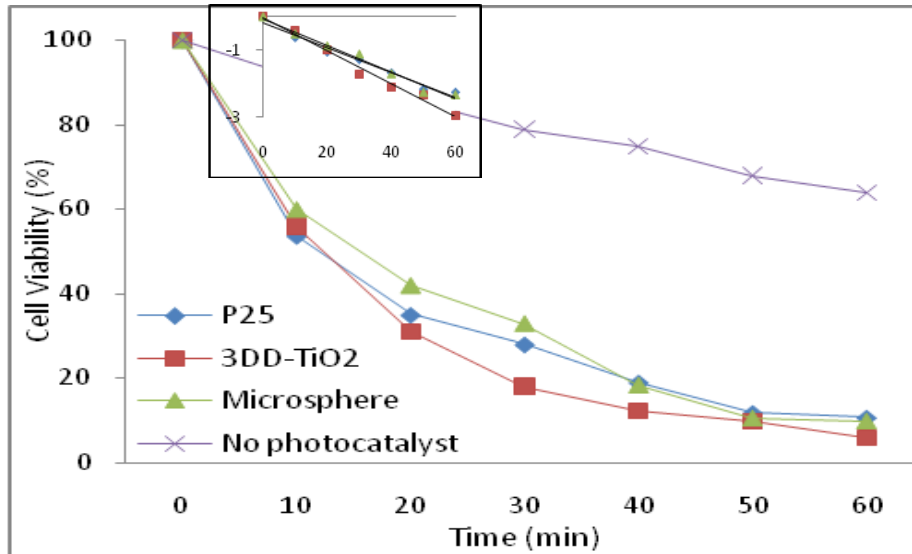
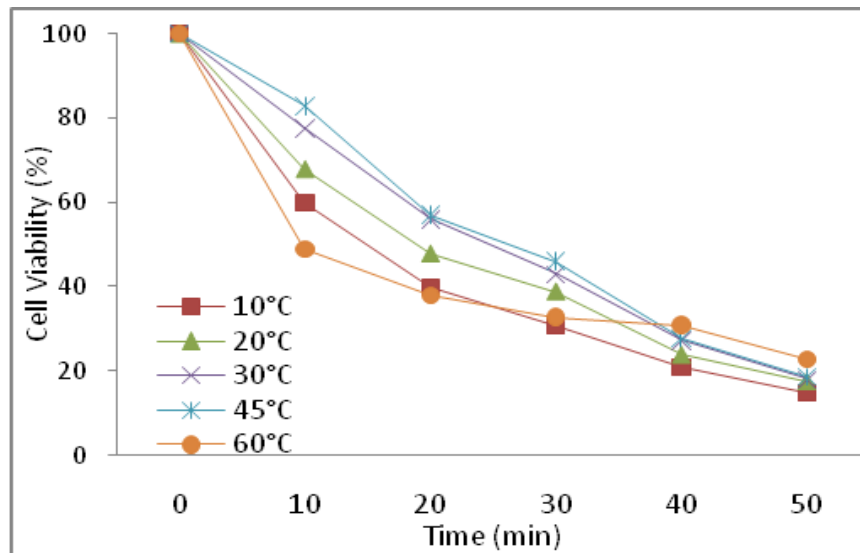


Figure 4: Comparison of results of treatment using P25, microsphere and 3DD-TiO<sub>2</sub> without UV radiation.



**Figure 5:** Comparison of results of treatment using P25, microsphere and 3DD-TiO2 under UV radiation. Inset depicts linearized plot of  $\ln$  [survival fraction] versus time, according to the Chick-Watson model.



**Figure 6:** Results of treatment using P25 under various temperatures.

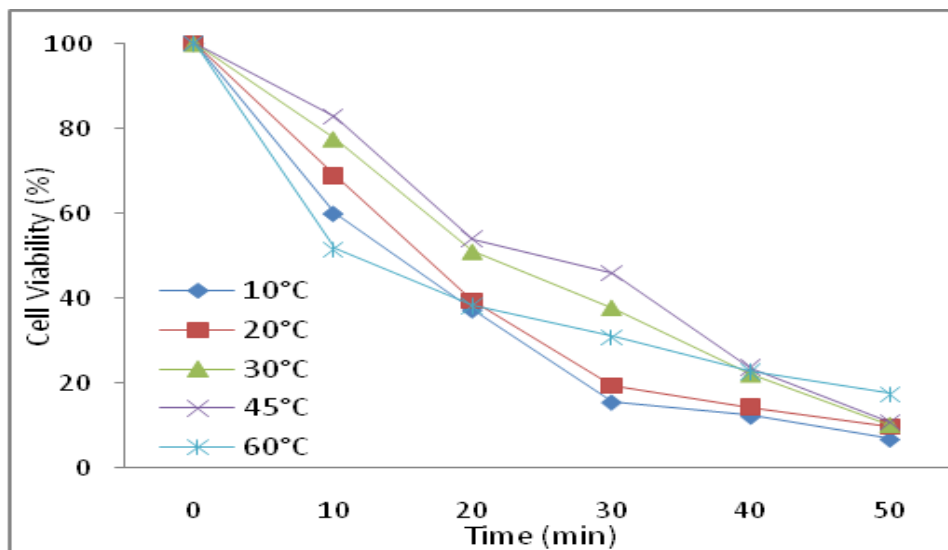


**Figure 7:** Results of treatment using 3DD-TiO<sub>2</sub> under various temperatures.

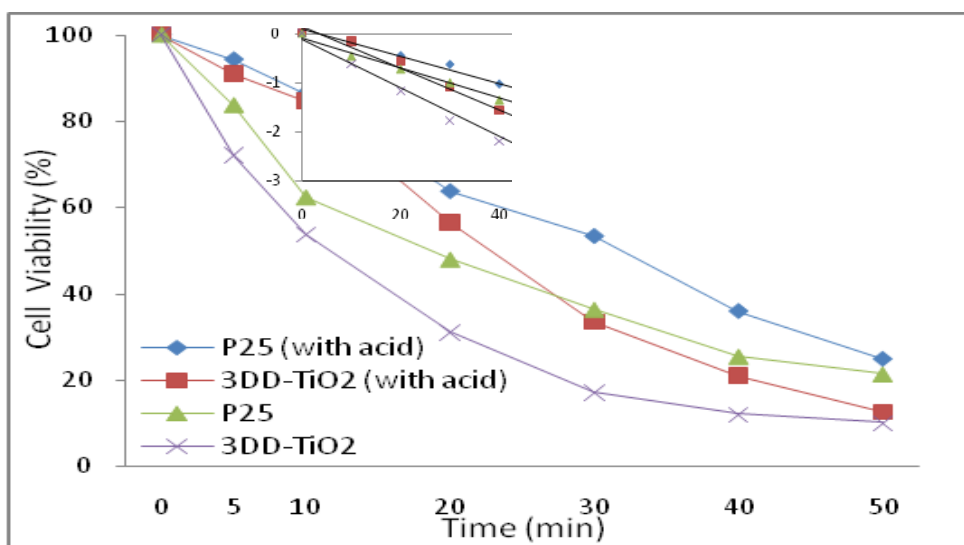


**Figure 8:** Results of treatment using P25 and 3DD-TiO<sub>2</sub>, with and without addition of humic acid. Inset depicts linearized plot of ln [survival fraction] versus time, according to the Chick-Watson model.

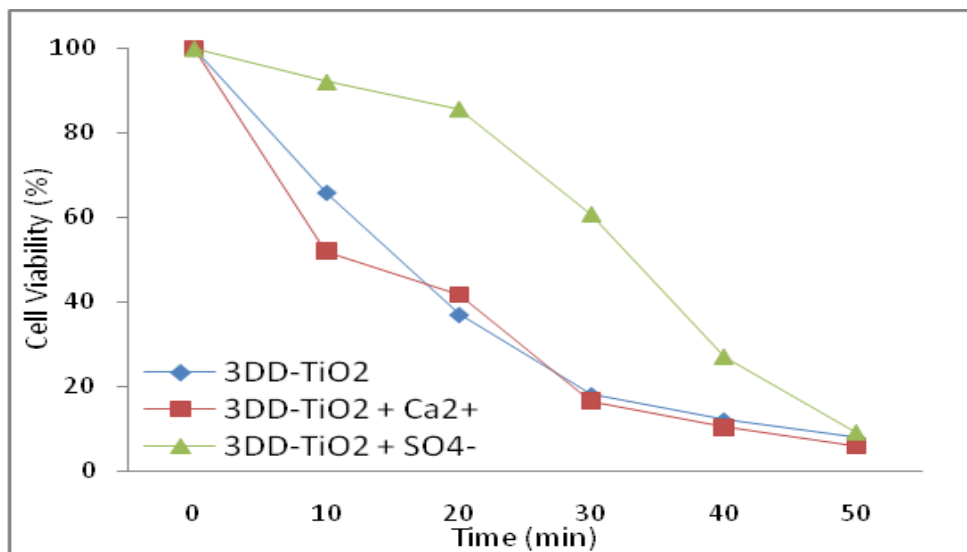


**Figure 9:** Results of treatment using 3DD-TiO<sub>2</sub> with ions. Inset depicts linearized plot of ln [survival fraction] versus time, according to the Chick-Watson model.

**Table 1:** Apparent first-order rate constants  $k$  of *E. coli* under different experimental conditions.

Experimental Condition	$k$ (min <sup>-1</sup> )
3DD-TiO <sub>2</sub> (100mg/L)	0.0494
P25 (100mg/L)	0.0369
Microsphere (100mg/L)	0.0401
3DD-TiO <sub>2</sub> + Humic acid	0.0428
3DD-TiO <sub>2</sub> + Ca <sup>2+</sup>	0.0533
3DD-TiO <sub>2</sub> + SO <sub>4</sub> <sup>2-</sup>	0.0427